Low-Power Gas Microbubble Detection Technology based on Acoustic Resonance

Manuel Rivera*, Edwin López, Silvina Cancelos and Carlos Marín

Dr. Manuel Rivera, Edwin López, Prof. Silvina Cancelos, Dr. Carlos Marín
SIL Technologies, LLC, Rincón, 00677, Puerto Rico
Email: manuel.rivera@siltechnologies.com

Prof. Silvina Cancelos, Edwin López
Bubble Dynamics Laboratory, Department of Mechanical Engineering, University of Puerto Rico - Mayagüez Campus, Mayagüez, 00681, Puerto Rico

Dr. Carlos Marín
Department of Engineering Science and Materials, University of Puerto Rico - Mayagüez Campus, Mayagüez, 00681, Puerto Rico

Keywords: bubble detectors, acoustic resonance, piezoelectrics

Abstract

A novel approach towards developing a micro-bubble detection technology based on using a PZT transducer to induce an acoustic resonance state within the system under investigation is here presented. The concept, originally proof-of-concept tested in a cylindrical acoustic resonant chamber, has proven to be able to detect single microbubbles with diameters in the range of 390 to 600 µm in a swine thigh, with either saline solution or sheep blood as the medium in the bubble guide. It has shown to be extremely adaptable, capable of accommodating industrial pipes as well as biological specimens, resilient and extremely energy efficient, able to detect micro-bubbles with as little as 0.8 mW and potentially less.

Gas bubble detection is a critical component of the instrumentation needed in many industrial and medical processes as well as in fundamental research of two-phase flow systems, cavitation phenomena, sonochemistry, sonoluminescence, and even biophysics of gene transport [1-9]. Real-time information and detection of bubble populations are required for most filling operations in

the paint, food, detergent, and cosmetic industries were bubbles can compromise the final product [10, 11]. In Ecology and Climate Science, bubble detection technology is required to understand the flux of greenhouse gasses such as methane and carbon dioxide between the ocean and the atmosphere [12-16]. In the field of medicine, the demand for air bubble detectors is surging, as healthcare practitioners are increasingly using these devices in combination with infusion pumps, dialysis equipment, and other fluid management applications. It is estimated that by 2030 the world market for air bubble detectors will be around $200 million [17].

Bubble detection based on ultrasonic attenuation is by far the most common technique of current bubble detectors [18-22]. Ultrasonic bubble detectors are effective and convenient in applications when bubbles no smaller than around 800 μm need to be detected in tubings of a specific size. But for the detection of smaller bubbles and in systems more complicated than a vinyl tube, the power requirements steeply increase, and the overall hardware and setup becomes prohibitively complicated and costly [11, 16, 22].

We report on our recent results obtained from a novel bubble detection technology based on acoustic resonance that accommodates any system of any geometry through which bubbles may travel and need to be detected. Besides its high degree of adaptability, it has extremely low power requirements, it is highly portable and highly sensitive; detecting bubbles as small as $3x10^{-5}$ mL. The technology uses a ring, or segments of a ring, piezoelectric (PZT) transducer attached and coupled around the girth of an object. Electrical current, voltage, current-to-voltage phase lag, and frequency across the PZT are constantly measured and recorded. Acoustic resonance of the coupled PZT – load system is correlated to the electric resonance measured in the PZT. The concept was originally developed in a resonant acoustic chamber designed by our group [9, 23, 24]. Briefly, this acoustic chamber consists of a cylindrical borosilicate glass with diameter of 95 mm

and 300 mm in length, sandwiched between two square acrylic flanges were all required fittings for fluid and bubble injection are installed. An 8mm vinyl tube runs the length of the glass cylinder where bubbles are injected, and the rest of the chamber is filled with degassed water. A ring PZT is attached to the outer surface of the cylindrical glass. **Figure 1A** shows a schematic drawing of the vertical cross-section of the acoustic resonance chamber. A frequency scan is conducted in order to establish the acoustic resonance of the system. Once established an acoustical pressure standing-wave is generated inside the cavity enclosed by the PZT. The same figure also shows the vertical acoustic pressure distribution created when the transducer is driven at the resonance frequency. The large peak located at the height of the PZT represents the main anti-node of the standing wave and is seen accompanied by several much smaller "satellite" antinodes. Any appearance of an inhomogeneity such as a gas bubble will perturb the resonance state which should reflect in the recorded electric signals from the PZT.

In **Figure 1B** the electric analogous of the resonance state is shown. Figure 1B shows the conductance measured across the PZT as function of frequency. Driving the PZT at the frequency at which conductance is maximum will put the system in mechanical resonance and the pressure standing wave of Figure 1A is obtained. Slug flow with a large Taylor bubble of around 7 mm in size was introduced into the chamber through the vinyl tube and positioned at the center of the cylindrical chamber. After this, a frequency scan of conductance was performed. The results, shown in Figure 1B, reveal that the conductance peak obtained without the bubble, shifts towards higher frequency and reduces in magnitude when the bubble is inside the chamber at the height of the PZT. When a constant voltage amplifier supplies the power, this change in conductance due to the presence of the bubble will manifest as a current drop across the PZT and this constitutes the bubble detection mechanism.

This concept was tested on a more challenging system to test for its adaptability, resilience, and sensibility. First of all, instead of a complete ring PZT, only two ring segments, each shorter than a semicircle, where used in order to provide flexibility to attach to different geometries and sizes. Secondly, these PZT ring segments were wrapped around a freshly cut swine thigh supplied by a local meat distributor. The segments were kept in place with an elastic band around them and ultrasonic gel was used to fill out the gaps between the PZT and the swine meat. The ring segments were then serially connected, and operation as described for the acoustic chamber was carried out. **Figure 2A** shows a schematic of the swine thigh with the PZT attached. A frequency scan, as previously described, was carried out to determine the frequency of maximum conductance. The PZT was driven continuously at the electrical resonant frequency and measurements with a hydrophone were done to determine whether the swine thigh was in a mechanical resonant state. As seen in Figure 2A, a clear standing-wave profile with clear nodes and antinodes was generated inside the swine thigh. Compared to the glass acoustic chamber, the secondary antinodes, those not at the height of the PZT, are much more pronounced than those in the acoustic chamber.

Once we confirmed that the acoustic pressure standing-wave was generated inside the swine thigh, and that the equivalence between the mechanical resonant state of the PZT-swine thigh coupled system and the electric resonant state of the PZT hold as it did for the glass cylinder, bubble detection tests in the swine thigh were performed. The experimental setup required for this task can be seen in **Figure 2B**. Briefly, a freshly cut swine thigh with a blood-mimicking prosthetic vessel transversely positioned serving as a bubble guide, was vertically hanged as to allow an injected bubble to travel the length of the vessel by buoyancy. The end of the vessel sticking out of the bottom of the swine thigh was connected to a pressure-controlled bubble

capillary bubble generator, while the upper extreme is submerged in a water-filled "outlet pool" (Figure 2B) where any injected bubble is discharged and recorded for image analysis. The 50 fps high-speed Cameras 1 and 3 in Figure 2B record injected and discharged bubbles at the pool outlet respectively. Finally, the two-segment PZT serially connected is attached to the swine thigh as seen in the figure. The PZT is powered by a Keysight 33500B wave generator amplified by an E&I 1040L RF power amplifier which increases output power by 55dB. The RMS voltage and current across the PZT is monitored while the PZT is operated at the resonant frequency at different powers. Typical voltage RMS data of the unperturbed system in the resonant state is shown in **Figure 2C**. As expected, the RMS voltage value randomly fluctuates around some average value determined by the supplied power and conductance of the PZT.

With the experimental setup of Figure 2B in place, bubble detection tests were carried out by injecting bubbles into the artificial blood vessels in a controlled manner and searching for any changes in the measured RMS voltage across the PZT. Again, the hypothesis being that a bubble traveling along the swine thigh which is in mechanical resonance will perturb the resonant state and this will reflect on the electric resonant state in the form of a change in the RMS behavior. **Figure 3A** shows the voltage RMS value as a function of time of two consecutive tests, one powered at 20 mW and the other 8 mW and each with a 575 μm in diameter bubble injected. Saline solution 0.9%wt was used as the liquid medium filling the vessel bubble guide and the outlet pool. The experiment is programmed to begin the data collection process at precisely the instant the bubble detaches from the capillary tip. Initially, the bubble will travel a segment of the bubble guide between the bubble generator and the swine thigh. During this time, which depends on the bubble size, the RMS should behave similar to Figure 2C, and at some point along the trajectory inside the swine thigh, an RMS perturbation should be observed. In both consecutive

tests shown in Figure 3A, we observe a fluctuating RMS baseline for about the first 4 seconds, at which point in time a clear, well defined and well above noise level RMS signal can be discerned. Several key observations are worth highlighting. First, both consecutive tests present an onset of the signal perturbation at exactly the same instant in time, indicating that the measurement is reliable and surprisingly reproducible when considering that the system is a hanging dead swine thigh. Secondly, the baseline value and short-term behavior can vary significantly, likely due to being powered by only 20 mW. However, reproducible features consisting of valleys and peaks consistently appearing at the same instant in the signal are visible. However, one of the most surprising observations was the fact that the onset of the bubble signal consistently coincide with the moment the bubble reached the point in the prosthetic vessel that entered inside the swine thigh, and completely died out at the moment the bubble appeared on the other side right before reaching the outlet pool. Considering that the moment the microbubble enters the approximately 38 lbs. swine thigh is at least 1 ft away from the PZT and that with 20mW the resonant state is sensitive enough to generate a clear detection signal is quite unprecedented.

To further test the detection system capabilities, smaller single bubbles (410 and 420 μm in diameter) were generated and injected into the swine thigh through the bubble guide with the PZT operated at resonance with 3mW supplied power. The results of two consecutive tests of this type are presented in **Figure 3B**. Other trials under the same experimental conditions yielded similar results. As in the previous experiments, a clear signal can be observed as soon as the bubble entered the swine thigh with attributes that consistently appeared in all the experiments and that lasted the bubble's entire time of flight inside the swine. The results of both set of experiments presented in Figures 3A and 3B suggest that the particular form the voltage RMS signal obtains is related to the pressure standing wave profile (Figure 2A) since it also consists of

a series of peak and valleys distributed along the entirety of the swine thigh. Following the set of

experiments presented in figure 3, we proceeded to test detection capabilities applying only 0.8

mW to the PZT, the lowest power possible allowed by the generator. In each test a single bubble,

with diameters between 402 and 395 μm, was injected with PZT operated at resonance and the

RMS voltage was recorded. Four consecutive tests under these experimental conditions are

shown in **Figure 4A**. Just as in previous cases, a distinguishable signal with reproducible features

appear in the voltage RMS data as soon as the test single bubble enters the swine. Arrows in the

figure point out the signal's features that consistently appear in all four tests. Baseline RMS

appears to fluctuate more than in previous cases, but this is expected given that the supplied

power is only 0.8 mW. Since how the presence of the bubble affects the pressure profile as it

travels along the swine thigh and goes through each of the antinodes would depend on many

factors such as bubble size, bubble speed, power applied and many particularities of the swine

meat that change with time and vary drastically from specimen to specimen, it is not surprising

that the form of the signal we observed considerably varied in different sets of experiments.

However, it is clear by looking at Figures 3A, 3B and 4A, that the distinguishable attributes of

the RMS signal are reproducible to a high degree proving that there is a finite set of factors that

predetermined the form of the signal. In the case presented in Figure 4A, although the main peaks

in the RMS data are equally reproducible, the baseline fluctuations observed at both extremes in

all cases makes it difficult to determine the duration or length of the signal. In order to determine

the time interval in which the signal is present, a numerical approximation of the data's derivative

was calculated. The results allowed for a single scale comparison and are presented in **Figure 4B**.

As seen in the figure, all the reproducible features observed in the RMS signal are confirmed in

its derivative. However, a clearer determination of the signal onset, at t=5.95s, can be established

as it is when the first signature feature consistently appearing in all tests occurs. Similarly, at

t=20.56s the RMS derivative quickly settles into fluctuations around 0 V/s and can be considered the end of the signal. Overall, the derivative shown in Figure 4B definitively proves that the apparatus is detecting single microbubbles all along the length of the swine thigh, which again is at least 1 ft long, while consuming only 0.8 mW. As a final test, a 600 μm single bubble was injected into the swine thigh through the prosthetic vessel, only in this instance, the vessel was filled with defibrinated sheep blood purchased from HemoStat Laboratories The voltage RMS obtained in this experiment can be seen in **Figure 4C**, where the PZT is driven with 3 mW. Same as in the cases where saline solution was used, the bubble traveling along the swine thigh through the sheep blood medium generates a perturbation in the acoustic pressure standing wave inside the swine thigh that manifests in the recorded RMS voltage. The drag force experienced by the bubble is higher in blood than in saline solution and hence the signal in the RMS chart appears much later in time than in the previous cases. The signal-to-noise ratio in the blood experiment is comparable with that of saline solution and a clear signal can be observed with onset occurring around t=19s and a form that resembles more the pressure profile observed in Figure 2A. However, it is extremely difficult at this point to derive any exact association between the voltage RMS signal observed and the pressure profile generated at resonance given that the exact pressure profile is likely to change with each swine thigh and maybe day by day. Our work is currently directed towards understanding the relationship between the pressure profile and characteristics of the RMS signal.

In conclusion, we have reported on a novel approach to developing a bubble detection technology based on using a PZT transducer to induce an acoustic resonance state within the system under investigation. Based on the hypothesis that if the mechanical resonant state of the system corresponds to the electric resonance state of the PZT then the appearance of any inhomogeneity

such as a microbubble would reflect on the electric response by interacting with the standing wave. The concept was tested and confirmed in a cylindrical acoustic resonant chamber. Moreover, the technology proved to be able to detect single microbubbles in the range of 390 to 600 μm in a swine thigh, with either saline solution or defibrinated sheep blood as the medium in the bubble guide. Absolute limits of bubble size sensitivity have not been established and based on the results here presented, the bubble size range it can detect is likely much larger. The major innovative benefits the technology has is its high degree of adaptability, as it can accommodate industrial pipes or a biological specimen, consistency, reliability and that it can be operated with as little as 0.8 mW (potentially less, the limit has not been established). Additionally, the spatial range of detection covered the entire swine thigh in 100% of the cases, and therefore more work is required to determine how large is the range of detection.

References:

1. K. Yasui, *Acoustic Cavitation and Bubble Dynamics,* Springer International Publishing, Cham, Switzerland **2018**.

2. A. Prosperetti, in *Sonochemistry and Sonoluminescence. NATO ASI Series (Series C: Mathematical and Physical Sciences)*, Vol. 524 (Eds: L. A. Crum, T.J. Mason, J. L. Reisse, K. S. Suslick), Springer Science+Business Media, Dordrecht, Netherlands **1999**, pp. 39.

3. Y. F. Ronald, *Sonoluminescence*, CRC Press, Boca Raton, FL, USA, **2005**.

4. A. van Wamel, K. Kooiman, M. Harteveld, M. Emmer, F. J. ten Cate, M. Versluis, N. de Jong, *J. Control. Release*. **2006** *112*, 2.

5. Z. Fan, R. E. Kumon, C. X. Deng, *Ther. Deliv*. **2014**, *5,* 4.

6. W. J. Galloway, *J. Acoust. Soc. Am*. **1954**, *26*, 5.

7. A. A. Atchley, L. A. Crum, in *Ultrasound. Its Chemical, Physical, Biological Effects*, (Eds: K. Suslick), VCH, New York, NY, USA **1988**, Ch.1.

8. T. G. Leighton, *The Acoustic Bubble*, Academic Press, San Diego, CA, USA **1994**.

9. S. Cancelos, F. J. Moraga, R. T. Lahey, W. Shain,R. H. Parsons, *J. Acoust. Soc. Am*. **2010** *128*, 2726.

10. R. M. Detsch, R. N. Sharma, *Chem. Eng. J*. **1990**, *44,* 3.

11. T. G. Leighton, D. G Ramble, A. D. Phelps, C. L. Morfey, P. P. Harris, *Acta Acust. united with Acust*. **1998** *84*, 801.

12. A. Watson, in *The Global Carbon Cycle. NATO ASI Series (Series I: Global Environmental Change)*, Vol. 15 (Eds: M. Heimann), Springer, Berlin, Germany **1993**, pp. 397.

13. T. G. Leighton, presented at 24th Int. Congr. Sound Vib, London, UK, July, **2017**.

14. D. M. Farmer, S. Vagle, A. D. Booth, *J. Atmos. Ocean. Technol*. **1998** *15*, 5.

15. S. Vagle, D. M. Farmer, *IEEE J. Ocean. Eng*. **1998** *23*, 3.

16. N. Breitz, H. Medwin, *J. Acoust. Soc. Am*. **1989** *86*, 739.

17. Transparency Market Research, Report on the global air bubble detectors market, https://www.transparencymarketresearch.com/air-bubble-detector-market.html, accessed: July, 2020.

18. T. G. Leighton, *Environ. Eng*. **1994** *7*, 9.

19. E. G. Tickner, in *Developments in Cardiovascular Medicine*, Vol 13 (Eds: H. Rijsterborgh), Springer, Dordrecht, Netherlands **1981**, pp. 461.

20. H. Medwin, *Ultrasonics.* **1977** *15*, 1.

21. L. A. Crum, *J. Acoust. Soc. Am.* **1980**, *68*, 203.

22. T. G. Leighton, A. D. Phelps, D. G. Ramble, D. A. Sharpe, *Ultrasonics.* **1996** *34*, 6.

23. S. Cancelos, C. J. Marin, A. Saavedra, (University of Puerto Rico), *US Patent 10,376,244 B1*, **2015**.

24. F. I. Valentin, S. Cancelos, *Proceedings of the ASME 2012 Summer Bioengineering Conference. ASME 2012 Summer Bioengineering Conference, Parts A and B* Fajardo, Puerto Rico, USA June **2012** pp. 819.

.
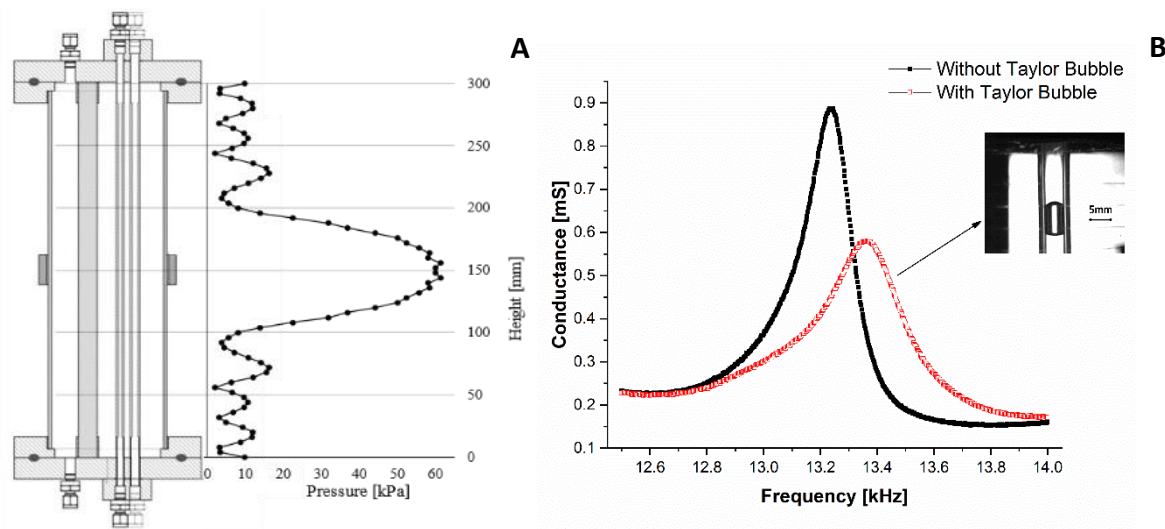
Figure 1. A) Schematic drawing of a cross-section of the acoustic resonance chamber along the pressure profile when chamber is in the resonant state. B) The conductance of the PZT as function of frequency. Peaks correspond to electric resonance frequency. Black curve represents the chamber's native state and the red curve corresponds to the chamber with a Taylor bubble inside.
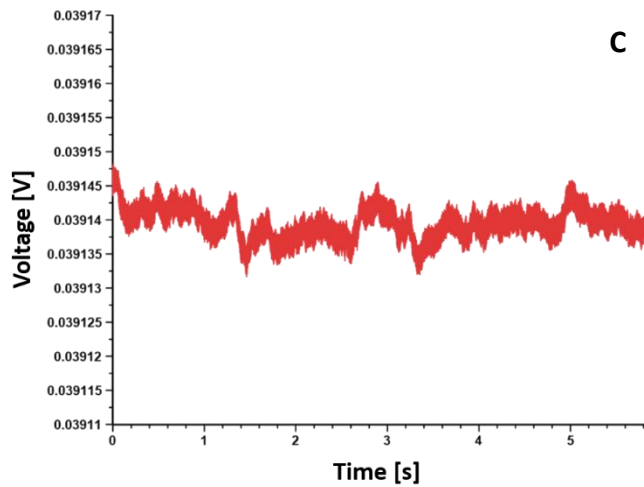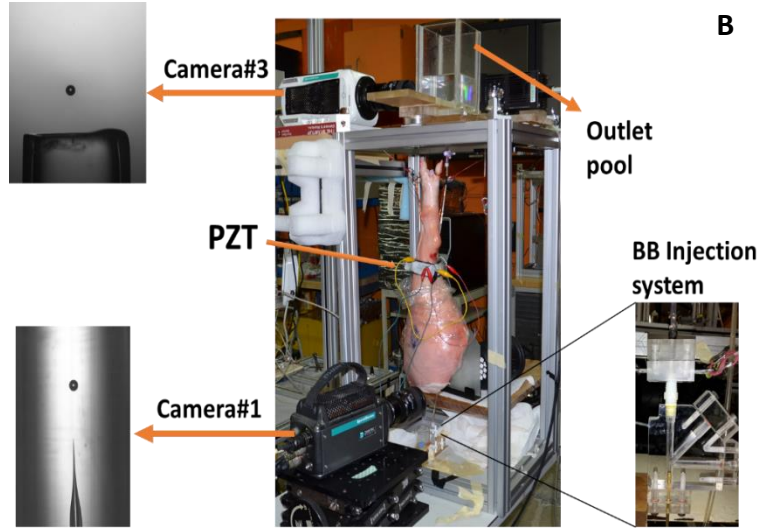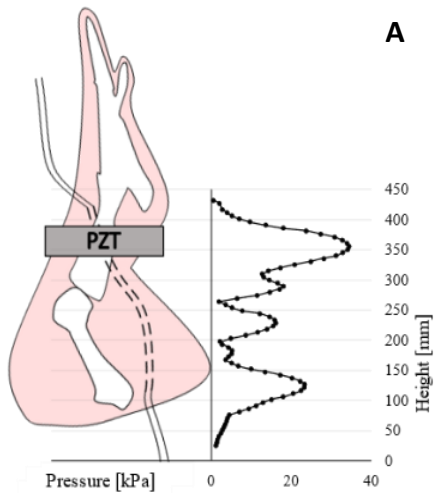
Figure 2. A) schematic of the swine thigh with the PZT attached and the pressure standing-wave profile generated within when the PZT is operated at its electric resonance frequency. B) Photograph of the experimental setup required for the bubble detection experiments. C) RMS of voltage monitored across the powered PZT with no bubbles present.
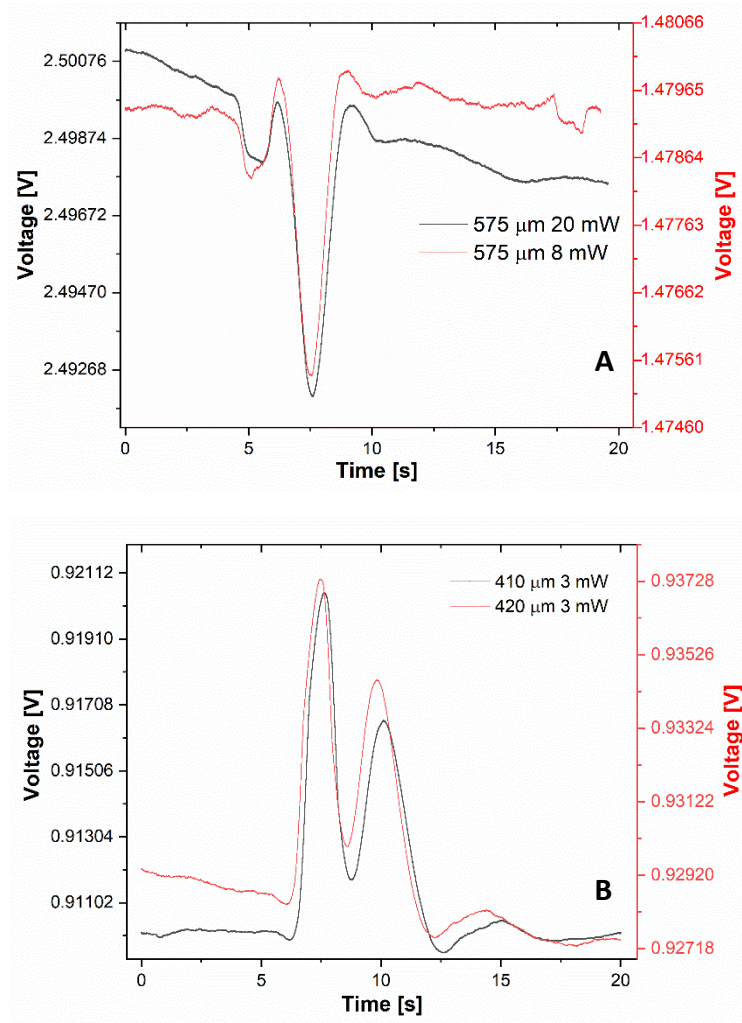
Figure 3. A) Two conecutive tests showing the voltage RMS as function of time using a 575 μm single bubble and two different powers and B) RMS signal of a 410 and 420 μm bubbles powered at 3mW each; the 10 nm is enough to slightly shift the peak of the largest bubble to the left due to having higher speed
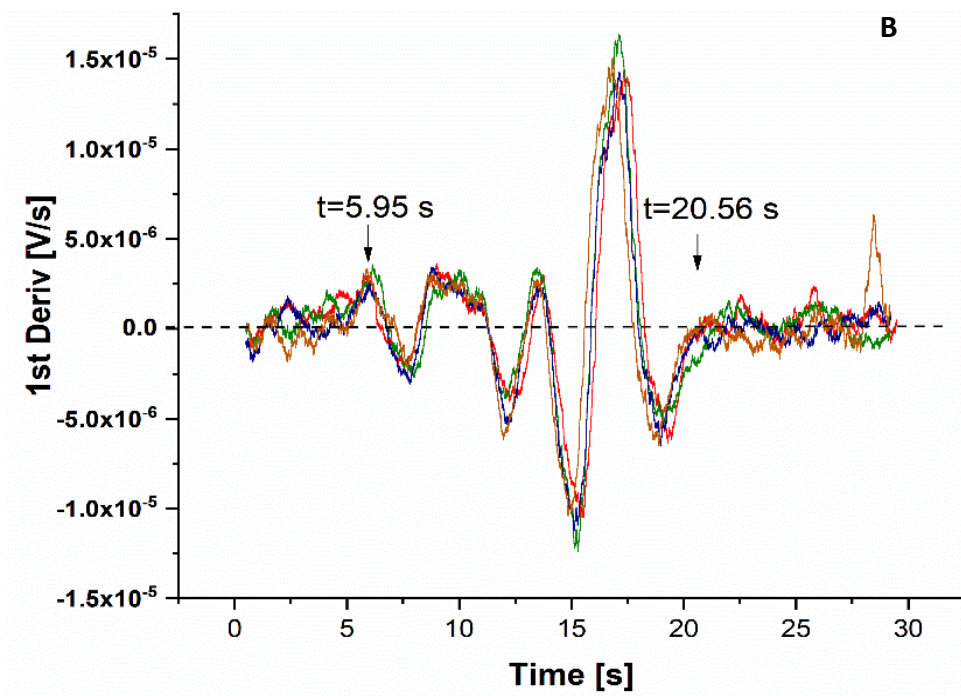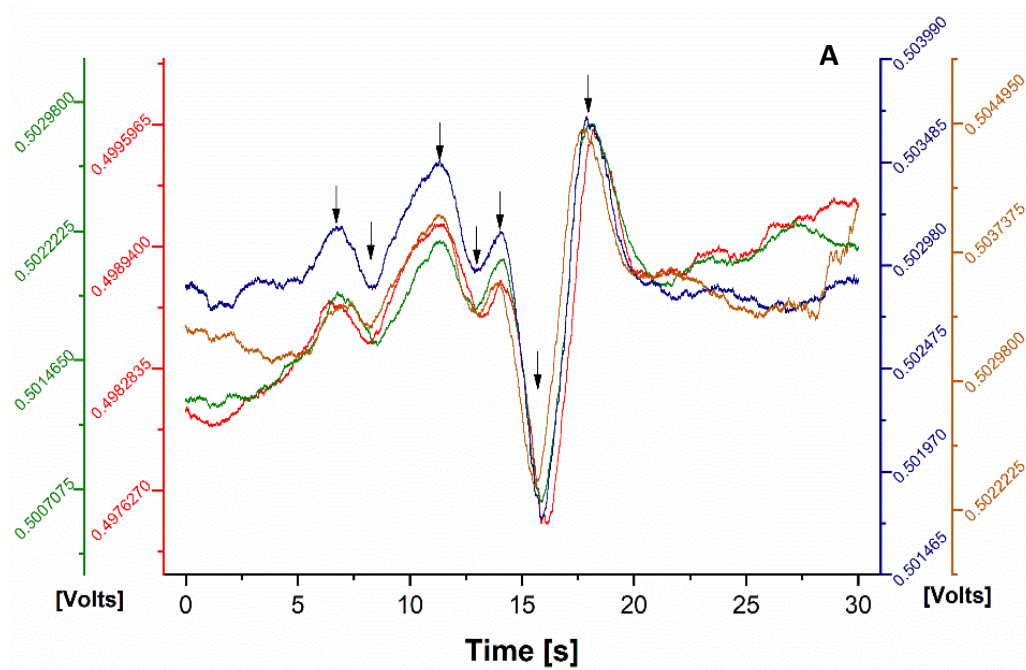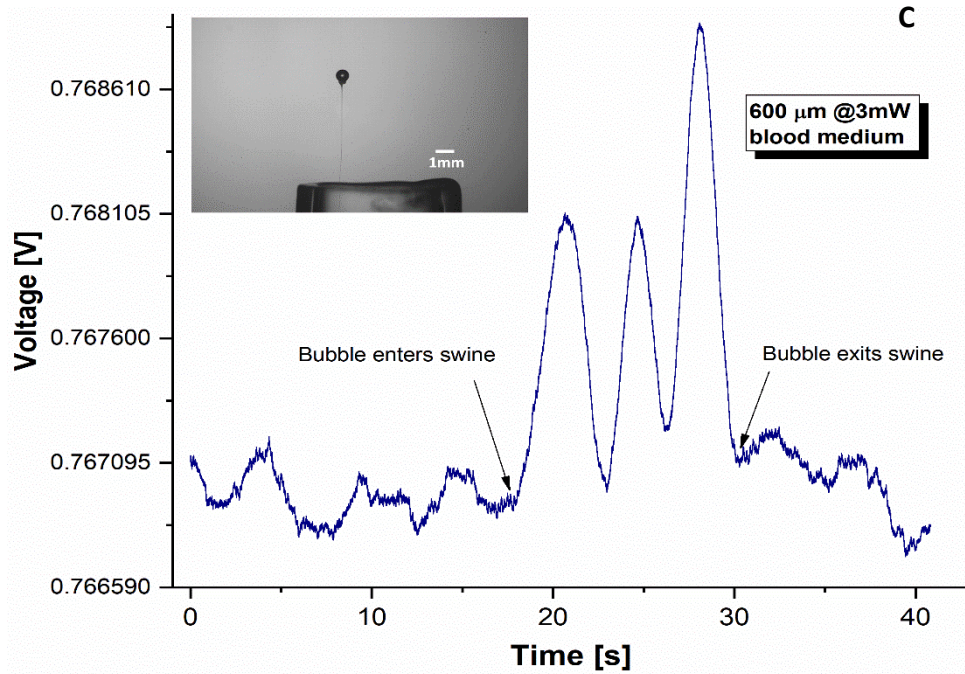
Figure 4. A) Four consecutive detection tests performed at 0.8 mW on bubbles around 400 µm in diameter. Arrows indicate reproducible features that constitute the detection signal. B) First derivative numerical approximation of the RMS data in A). C) 600 µm single bubble detection test using defibrinated sheep blood instead of saline solution and operated at 3 mW.